

Thermoelectric efficiency in multiterminal quantum thermal machines from steady-state density functional theory

N. Sobrino,^{1,*} R. D'Agosta,^{1,2,†} and S. Kurth^{1,2,3,‡}

¹*Nano-Bio Spectroscopy Group and European Theoretical Spectroscopy Facility (ETSF),
Departamento de Polímeros y Materiales Avanzados: Física,
Química y Tecnología, Universidad del País Vasco UPV/EHU,
Avenida de Tolosa 72, E-20018 San Sebastián, Spain*

²*IKERBASQUE, Basque Foundation for Science, Plaza de Euskadi 5, E-48009 Bilbao, Spain*

³*Donostia International Physics Center, Paseo Manuel de Lardizabal 4, E-20018 San Sebastián, Spain*

(Dated: May 11, 2023)

The multi-terminal generalization of the steady-state density functional theory for the description of electronic and thermal transport (iq-DFT) is presented. The linear response regime of the framework is developed leading to exact expressions for the many-body transport coefficients and thermoelectric efficiency purely in terms of quantities accessible to the framework. The theory is applied to a multi-terminal interacting quantum dot in the Coulomb blockade regime for which accurate parametrizations of the exchange-correlation kernel matrix are given. The thermoelectric efficiency and output power of the multi-terminal system are studied. Surprisingly, the strong-interaction limit of these quantities can be understood in terms of the non-interacting one.

I. INTRODUCTION

In recent decades, electronic transport through nanoscale devices, even down to the size of single molecules, has attracted increasing scientific and technological interest.^{1,2} The main motivation for this interest is the reduction of the dimensions of active electronic devices, e.g., control of electronic currents at ever smaller scales. However, at these small scales, heat management becomes crucial for reliable device operation. Also, one may aim to harness thermal energy by conversion to electrical currents in thermoelectric devices.^{3–9} Therefore it is important to deal with both electrical and thermal transport on equal footing. Although two-terminal setups have been the focus of most investigations, the exploration of thermoelectric transport in multi-terminal devices^{10–18} has started more recently due to the potential added benefits of these more intricate designs, to, e.g., separate heat and electrical transport.

For non-interacting electrons, an adequate framework to describe both electronic and heat transport in the steady state is the Landauer-Büttiker (LB) formalism^{19,20} which treats transport essentially as a scattering problem. On the other hand, to describe the currents through an interacting region attached to non-interacting leads, we have the Meir-Wingreen formula²¹, which expresses the currents in terms of the many-body spectral function.

For an ab-initio modeling of materials, density functional theory (DFT)²² has become an indispensable tool, mainly due to its reasonable balance between accuracy and numerical efficiency. While DFT was originally formulated for (thermal) equilibrium, a combination of DFT with the LB formalism has widely been used to model both electronic and heat transport through, e.g., single molecules^{23–28}. However, one has to keep in mind that standard DFT is not designed to describe out-

equilibrium physics such as electronic or thermal transport. While in special circumstances this may be enough to capture, e.g., linear transport coefficients^{29–32}, in general extensions of the theory are required. One such possible extension for the description of transport is steady-state DFT (or i-DFT)³³ which adds to the basic quantity of standard DFT and LB-DFT, the density, another fundamental variable, the steady-state electronic current. This framework has been used to describe transport through model systems, including strongly correlated ones^{34–38} and has also been formulated to deal with multi-terminal systems.³⁹

In more recent work⁴⁰, an extension of steady-state DFT, dubbed iq-DFT, has been suggested which besides the electronic (particle) current also allows for the description of (electronic) heat or energy currents. In the present work, we extend iq-DFT to systems connected to an arbitrary number of leads (Sec. II) with explicit development of the linear-response regime. In Sec. III A, the formalism is applied to the single-impurity Anderson model (SIAM) in the Coulomb blockade regime for which we present the exchange-correlation (xc) kernel of linear response. This allows to study all the linear transport coefficients (electrical and thermal conductances, Seebeck coefficients, etc.) solely in terms of iq-DFT quantities. For the numerical results (Sec. III B) we focus on the multi-terminal efficiency of the SIAM viewed as a thermal machine and we show explicitly that in the strong-interaction limit this quantity strictly reduces to its non-interacting counterpart. Finally, we present our conclusions in Sec. IV.

II. MULTI-TERMINAL IQ-DFT

We consider a general electronic transport setup as depicted in Fig. 1, where \mathcal{N} (semi-infinite) electrodes are coupled to a central (molecular) region (C) subject to an

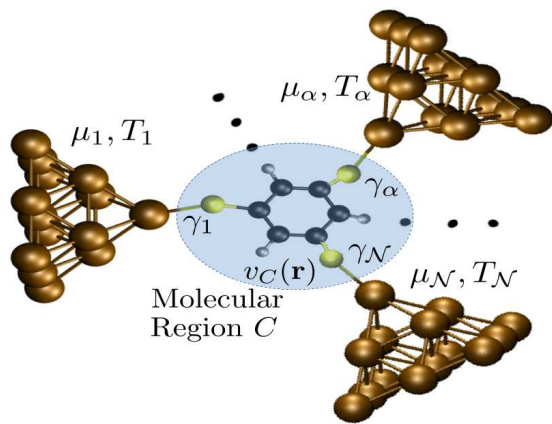


FIG. 1. Schematic drawing of a multi-terminal nanoscale junction. A molecular region C at gate potential $v_C(\mathbf{r})$ is coupled to \mathcal{N} leads at chemical potentials $\mu_\alpha = \mu + V_\alpha$ and temperatures $T_\alpha = T(1 + \Psi_\alpha)$.

electrostatic potential $v_C(\mathbf{r})$ which vanishes deep inside the electrodes (leads). While the electrodes are assumed to be at *local* equilibrium characterized by temperatures T_α and chemical potentials μ_α ($\alpha = 1, \dots, \mathcal{N}$), the total system is considered to be in a non-equilibrium steady state. For convenience we also define both an *equilibrium* temperature and chemical potential as $T = \frac{1}{\mathcal{N}} \sum_\alpha T_\alpha$ and $\mu = \frac{1}{\mathcal{N}} \sum_\alpha \mu_\alpha$, respectively, such that the lead temperatures $T_\alpha = T(1 + \Psi_\alpha)$ can be expressed in terms of thermal gradients Ψ_α while the chemical potentials $\mu_\alpha = \mu + V_\alpha$ are written in terms of DC biases V_α . From these definitions of μ and T it follows that $\sum_\alpha V_\alpha = 0$ and $\sum_\alpha \Psi_\alpha = 0$, respectively.

The non-equilibrium steady state of the system is characterized by the electronic density $n(\mathbf{r})$ in region C , as well as two sets of steady currents: (a) the electronic and energy currents (I_α and W_α , respectively) flowing from lead α to region C , or (b) the corresponding electronic and heat currents (I_α and Q_α , respectively). These currents are related through

$$W_\alpha = Q_\alpha + \mu_\alpha I_\alpha, \quad (1)$$

and the multi-terminal iq-DFT approach described below can equivalently be formulated in terms of both fundamental current variables (a) or (b).

In the following, we adopt the sign convention that currents flowing into the central region C are positive. Due to charge and energy conservation, we have $\sum_\alpha I_\alpha = 0$, $\sum_\alpha W_\alpha = 0$, while from Eq. (1) we obtain for the heat currents $\sum_\alpha Q_\alpha = -\sum_\alpha I_\alpha V_\alpha$. Furthermore, atomic units are used throughout. Energies are given in units of temperature unless otherwise noted.

The extension of the iq-DFT formalism⁴⁰ to multi-terminal setups can be formally established through the following theorem. Here, without loss of generality, we assume that the gradients and currents associated with

the \mathcal{N} th lead are expressed in terms of the gradients and currents of the other $\mathcal{N} - 1$ leads.

Theorem: There exists a one-to-one correspondence between the set of “densities” ($n(\mathbf{r}), I_1, Q_1, \dots, I_{\mathcal{N}-1}, Q_{\mathcal{N}-1}$) and the set of “potentials” ($v(\mathbf{r}), V_1/T, \Psi_1/T, \dots, V_{\mathcal{N}-1}/T, \Psi_{\mathcal{N}-1}/T$), for any finite temperature T and fixed electrostatic potential in the leads, in a finite region around $V_\alpha = 0$ and $\Psi_\alpha = 0$ for all $\alpha = 1, \dots, \mathcal{N} - 1$. The proof of the theorem is analogous to the one presented in Ref. 41.

According to the theorem and under the usual assumption of non-interacting representability, there exists a unique set of Kohn-Sham (KS) potentials ($v_s(\mathbf{r}), V_{s,1}/T, \Psi_{s,1}/T, \dots, V_{s,\mathcal{N}-1}/T, \Psi_{s,\mathcal{N}-1}/T$) which in a noninteracting system reproduces the density $n(\mathbf{r})$ and currents ($I_1, Q_1, \dots, I_{\mathcal{N}-1}, Q_{\mathcal{N}-1}$) of the interacting system. Following the standard KS procedure, the xc potentials are defined as

$$v_{\text{Hxc}}[n, \mathcal{I}, \mathcal{Q}](\mathbf{r}) = v_s[n, \mathcal{I}, \mathcal{Q}](\mathbf{r}) - v[n, \mathcal{I}, \mathcal{Q}](\mathbf{r}), \quad (2a)$$

$$V_{\text{xc},\alpha}[n, \mathcal{I}, \mathcal{Q}] = V_{s,\alpha}[n, \mathcal{I}, \mathcal{Q}] - V_\alpha[n, \mathcal{I}, \mathcal{Q}], \quad (2b)$$

$$\Psi_{\text{xc},\alpha}[n, \mathcal{I}, \mathcal{Q}] = \Psi_{s,\alpha}[n, \mathcal{I}, \mathcal{Q}] - \Psi_\alpha[n, \mathcal{I}, \mathcal{Q}], \quad (2c)$$

for $\alpha = 1, \dots, \mathcal{N} - 1$, where $\mathcal{I} = (I_1, \dots, I_{\mathcal{N}-1})$ and $\mathcal{Q} = (Q_1, \dots, Q_{\mathcal{N}-1})$. The self-consistent coupled KS equations for the densities read ($f \equiv \int_{-\infty}^{\infty} \frac{d\omega}{2\pi}$ in the following)

$$n(\mathbf{r}) = 2 \sum_{\alpha=1}^{\mathcal{N}} \int f(\omega_{s,\alpha}) A_{s,\alpha}(\mathbf{r}, \omega), \quad (3a)$$

$$I_\alpha = 2 \sum_{\alpha'=1}^{\mathcal{N}} \int [f(\omega_{s,\alpha}) - f(\omega_{s,\alpha'})] \mathcal{T}_{s,\alpha\alpha'}(\omega), \quad (3b)$$

$$Q_\alpha = 2 \sum_{\alpha'=1}^{\mathcal{N}} \int [f(\omega_{s,\alpha}) - f(\omega_{s,\alpha'})] (\omega - \mu_{s,\alpha}) \mathcal{T}_{s,\alpha\alpha'}(\omega), \quad (3c)$$

where $\omega_{s,\alpha} = \frac{w - \mu_{s,\alpha}}{1 + \Psi_{s,\alpha}}$ with $f(z) = [1 + \exp(z/T)]^{-1}$ being the Fermi function and $\mu_{s,\alpha} = \mu + V_{s,\alpha}$ with the KS bias for lead α

$$V_{s,\alpha} = V_\alpha + V_{\text{xc},\alpha}[n, \mathcal{I}, \mathcal{Q}]. \quad (4)$$

In Eq. (3), the (partial) KS spectral function is defined as $A_{s,\alpha}(\mathbf{r}, \omega) = \langle \mathbf{r} | \mathcal{G}(\omega) \Gamma_\alpha(\omega) \mathcal{G}^\dagger(\omega) | \mathbf{r} \rangle$, with $\mathcal{G}(\omega)$ and $\Gamma_\alpha(\omega)$ the KS Green’s function and broadening matrices, respectively. Finally, the KS transmission function is $\mathcal{T}_{s,\alpha\alpha'}(\omega) = \text{Tr} \{ \mathcal{G}_s(\omega) \Gamma_\alpha(\omega) \mathcal{G}^\dagger(\omega) \Gamma_{\alpha'}(\omega) \}$.

A. Linear Response

Suppose we have a (multi-terminal) system in thermal equilibrium characterized by chemical potential μ and (common) temperature T and we are interested in the steady-state currents *to linear order* as external biases

and/or temperature gradients are applied to the system. In this linear regime, the relationship between the currents \mathbf{I} and the external potentials Φ reads

$$\mathbf{I} = \mathbf{L}\Phi \quad (5)$$

with the $2(\mathcal{N} - 1) \times 2(\mathcal{N} - 1)$ conductance matrix \mathbf{L} and the current and potential vectors defined as $\mathbf{I}^\top = (I_1, Q_1, \dots, I_{\mathcal{N}-1}, Q_{\mathcal{N}-1})$ and $\Phi^\top = (V_1/T, \Psi_1/T, \dots, V_{\mathcal{N}-1}/T, \Psi_{\mathcal{N}-1}/T)$, respectively. By construction, the matrix elements of \mathbf{L} are defined as

$$\mathbf{L}_{jk} = \left. \frac{\partial \mathbf{I}_j}{\partial \Phi_k} \right|_{\Phi=0} \quad (6)$$

and from Onsager's relation it follows that \mathbf{L} is symmetric, i.e., $\mathbf{L}_{jk} = \mathbf{L}_{kj}$ with $k, j \in \{1, \dots, 2(\mathcal{N} - 1)\}$.

Since by construction, the KS currents equal the interacting ones to *any* order, we may also linearize Eqs. (3b) and (3c) to obtain

$$\mathbf{I} = \mathbf{L}_s (\Phi + \Phi_{xc}) \quad (7)$$

where \mathbf{L}_s is the non-interacting (KS) linear response matrix. To linear order, the changes in the xc potentials can be written as

$$\Phi_{xc} = \mathbf{F}_{xc} \mathbf{I} = \mathbf{F}_{xc} \mathbf{L} \Phi \quad (8)$$

where we have defined the matrix of xc derivatives (which we alternatively denote the xc kernel) \mathbf{F}_{xc} as

$$\mathbf{F}_{xc} = \left(\begin{array}{ccccc} \frac{\delta V_{xc,1}}{\delta I_1} & \frac{\delta V_{xc,1}}{\delta Q_1} & \cdots & \frac{\delta V_{xc,1}}{\delta I_{\mathcal{N}-1}} & \frac{\delta V_{xc,1}}{\delta Q_{\mathcal{N}-1}} \\ \frac{\delta \Psi_{xc,1}}{\delta I_1} & \frac{\delta \Psi_{xc,1}}{\delta Q_1} & \cdots & \frac{\delta \Psi_{xc,1}}{\delta I_{\mathcal{N}-1}} & \frac{\delta \Psi_{xc,1}}{\delta Q_{\mathcal{N}-1}} \\ \vdots & \vdots & \ddots & \vdots & \vdots \\ \frac{\delta V_{xc,\mathcal{N}-1}}{\delta I_1} & \frac{\delta V_{xc,\mathcal{N}-1}}{\delta Q_1} & \cdots & \frac{\delta V_{xc,\mathcal{N}-1}}{\delta I_{\mathcal{N}-1}} & \frac{\delta V_{xc,\mathcal{N}-1}}{\delta Q_{\mathcal{N}-1}} \\ \frac{\delta \Psi_{xc,\mathcal{N}-1}}{\delta I_1} & \frac{\delta \Psi_{xc,\mathcal{N}-1}}{\delta Q_1} & \cdots & \frac{\delta \Psi_{xc,\mathcal{N}-1}}{\delta I_{\mathcal{N}-1}} & \frac{\delta \Psi_{xc,\mathcal{N}-1}}{\delta Q_{\mathcal{N}-1}} \end{array} \right) \Bigg|_{\mathbf{I}=0} \quad (9)$$

Combining Eqs. (5), (7), and (9), and using the fact that the V_α and Ψ_α are arbitrary, we arrive at the Dyson equation for the many-body conductance matrix \mathbf{L} expressed in terms of the KS one \mathbf{L}_s

$$\mathbf{L} = \mathbf{L}_s + \mathbf{L}_s \mathbf{F}_{xc} \mathbf{L}, \quad (10)$$

Note that Eq. (10) expresses the many-body conductance matrix completely in terms of iq-DFT quantities and may be rewritten as

$$\mathbf{F}_{xc} = \mathbf{L}_s^{-1} - \mathbf{L}^{-1}. \quad (11)$$

As a consequence of \mathbf{L} and \mathbf{L}_s being symmetric, also \mathbf{F}_{xc} must be symmetric, $(\mathbf{F}_{xc})_{kj} = (\mathbf{F}_{xc})_{jk}$

III. SINGLE IMPURITY ANDERSON MODEL

In this section, we apply our multi-terminal formalism to the simplest quantum thermal machine, namely, the

Single Impurity Anderson Model (SIAM). This system consists of a quantum dot that can hold up to two interacting electrons attached to \mathcal{N} non-interacting electron reservoirs. The Hamiltonian of the system reads

$$\hat{H} = \sum_{\sigma} v \hat{n}_{\sigma} + U \hat{n}_{\uparrow} \hat{n}_{\downarrow} + \sum_{\alpha k \sigma} \varepsilon_{\alpha k \sigma} \hat{c}_{\alpha k \sigma}^{\dagger} \hat{c}_{\alpha k \sigma} + \sum_{k \alpha \sigma} \left(t_{\alpha k} \hat{c}_{\alpha k \sigma}^{\dagger} \hat{d}_{\sigma} + H.c. \right). \quad (12)$$

The first two terms in Eq. (12) describe the isolated impurity, with v representing the on-site energy of the dot and U symbolizing the Coulomb interaction. The creation operators for electrons with spin σ ($\sigma = \uparrow, \downarrow$) in lead α and on the dot are denoted by $\hat{c}_{\alpha k \sigma}^{\dagger}$ and $\hat{d}_{\sigma}^{\dagger}$, respectively. The operators for the spin-resolved and the total density of electrons on the dot are given by $\hat{n}_{\sigma} = \hat{d}_{\sigma}^{\dagger} \hat{d}_{\sigma}$ and $\hat{n} = \hat{n}_{\uparrow} + \hat{n}_{\downarrow}$, respectively. The last term of the Hamiltonian (12) describes the tunneling between the dot and the leads, with couplings $\Gamma_{\alpha}(\omega) = 2\pi \sum_k |t_{\alpha k}|^2 \delta(\omega - \varepsilon_{k\alpha})$. We work in the wide band limit (WBL), i.e., the leads are assumed to be featureless and described by frequency-independent couplings $\Gamma_{\alpha}(\omega) = \gamma_{\alpha}$ (with $\alpha \in \{1, \dots, \mathcal{N}\}$). Without loss of generality, from here onwards we set the chemical potential $\mu = 0$.

A. Many body model for the construction of the exchange correlation kernel

In order to apply our multi-terminal iq-DFT framework, approximations for the xc potentials need to be constructed. Here we restrict ourselves to the linear-response regime and therefore we only need to construct the xc kernel matrix \mathbf{F}_{xc} .

As in previous works^{33,40}, a useful starting point for this construction is to write the interacting density on the dot as well as the (particle and heat) currents in the leads in terms of the many-body spectral function $A(\omega)$ as

$$n = 2 \sum_{\alpha=1}^{\mathcal{N}} \int \frac{\gamma_{\alpha}}{\gamma} f(\omega_{\alpha}) A(\omega) \quad (13a)$$

$$I_{\alpha} = 2 \sum_{\alpha'=1}^{\mathcal{N}} \frac{\gamma_{\alpha} \gamma_{\alpha'}}{\gamma} \int [f(\omega_{\alpha}) - f(\omega_{\alpha'})] A(\omega) \quad (13b)$$

$$Q_{\alpha} = 2 \sum_{\alpha'=1}^{\mathcal{N}} \frac{\gamma_{\alpha} \gamma_{\alpha'}}{\gamma} \int [f(\omega_{\alpha}) - f(\omega_{\alpha'})] (\omega - V_{\alpha}) A(\omega) \quad (13c)$$

with $\gamma = \sum_{i=1}^{\mathcal{N}} \gamma_{\alpha}$ and $\omega_{\alpha} = \frac{\omega - V_{\alpha}}{1 + \Psi_{\alpha}}$.

In order to proceed, we consider the following model for the many-body spectral function (MBM) which can be derived from the equations of motion technique⁴² and

provides a reasonably accurate approximation for $T/\gamma > 1$, i.e., for the Coulomb blockade regime³⁵

$$A(\omega) = \frac{\gamma \left(1 - \frac{\eta}{2}\right)}{(\omega - v)^2 + \frac{\gamma^2}{4}} + \frac{\gamma \frac{\eta}{2}}{(\omega - v - U)^2 + \frac{\gamma^2}{4}}. \quad (14)$$

For the non-interacting case with gate potential v_s , this spectral function becomes

$$A_s(\omega) = \frac{\gamma}{(\omega - v_s)^2 + \frac{\gamma^2}{4}}. \quad (15)$$

Then all the integrals for density and currents can be evaluated analytically⁴⁰ with the results

$$n^s = 1 - \frac{2}{\pi\gamma} \sum_{\alpha=1}^{\mathcal{N}} \gamma_{\alpha} \text{Im} [\psi(z_{s,\alpha})] \quad (16a)$$

$$I_{\alpha}^s = \frac{2\gamma_{\alpha}}{\pi\gamma} \left[\sum_{\alpha'=1}^{\mathcal{N}} \gamma_{\alpha'} (\text{Im} [\psi(z_{s,\alpha'})] - \text{Im} [\psi(z_{s,\alpha})]) \right] \quad (16b)$$

$$Q_{\alpha}^s = \frac{\gamma_{\alpha}}{\pi} \left[\sum_{\alpha'=1}^{\mathcal{N}} \gamma_{\alpha'} (\text{Re} [\psi(z_{s,\alpha})] - \text{Re} [\psi(z_{s,\alpha'})]) \right] \\ + \frac{\gamma_{\alpha}}{\pi} \sum_{\alpha'=1}^{\mathcal{N}} \left[\gamma_{\alpha'} \log \left(\frac{1 + \Psi_{s,\alpha}}{1 + \Psi_{s,\alpha'}} \right) \right] + (v_s - V_{s,\alpha}) I_{\alpha} \quad (16c)$$

where $z_{s,\alpha} = \frac{1}{2} + \frac{\frac{\gamma}{2} + i(v_s - V_{s,\alpha})}{2\pi T(1 + \Psi_{s,\alpha})}$ and $\psi(z)$ is the digamma function with general complex argument z .⁴³ Eqs. (16b) and (16c) can be expanded to linear order in the biases $V_{s,\alpha}$ and temperature gradients $\Psi_{s,\alpha}$ and the resulting integrals for the expansion coefficients can also be evaluated analytically. Writing $j = 2\alpha - 1$ ($j = 2\alpha$) for j odd (even) and similarly $k = 2\alpha' - 1$ ($k = 2\alpha'$) for k odd (even) we can express the non-interacting conductance matrix $\mathbf{L}_s(v_s)$ as function of v_s in the compact form

$$\mathbf{L}_{s,jk}(v_s) = \tilde{\gamma}_{jk} M_{jk}(v_s) \quad (17)$$

where the prefactor $\tilde{\gamma}_{jk}$ only depends on the couplings to the leads and can be written as

$$\tilde{\gamma}_{jk} = 2\gamma_{\alpha} \left(\delta_{\alpha,\alpha'} + \frac{\gamma_{\mathcal{N}} - \gamma_{\alpha'}}{\gamma} \right) \quad (18)$$

On the other hand, the coefficient $M_{jk}(v_s)$ depends on v_s and is defined as

$$M_{jk}(v_s) = \begin{cases} J_0(v_s) & \text{for both } j, k \text{ odd} \\ J_2(v_s) & \text{for both } j, k \text{ even} \\ J_1(v_s) & \text{otherwise} \end{cases} \quad (19)$$

where

$$J_l(v_s) = - \int \omega^l f'(\omega) \frac{\gamma}{(\omega - v_s)^2 + \frac{\gamma^2}{4}} \quad (20)$$

where $f'(\omega) = \frac{d}{d\omega} f(\omega)$. The integrals of Eq. (20) can also be computed analytically⁴⁰ with the results

$$J_0(v_s) = \frac{1}{2\pi^2 T} \text{Im}(i\psi^{(1)}(z_1^s)) \quad (21a)$$

$$J_1(v_s) = \frac{1}{2\pi^2 T} \text{Im}(z_0^s \psi^{(1)}(z_1^s)) \quad (21b)$$

$$J_2(v_s) = -\frac{\gamma}{4\pi^2 T} \text{Re}(z_0^s \psi^{(1)}(z_1^s)) + v_s J_1(v_s) + \frac{\gamma}{2\pi} \quad (21c)$$

where $z_0^s = \frac{\gamma}{2} + iv_s$, $z_1^s = \frac{1}{2} + \frac{z_0^s}{2\pi T}$ and $\psi^{(1)}(z)$ is the trigamma function.⁴³

Due to the simple structure of the model many-body spectral function of Eq. (14), we can now express the corresponding *interacting* conductance matrix in terms of quantities obtained for the non-interacting case as

$$\mathbf{L}_{jk}(v) = \tilde{\gamma}_{jk} \left[\left(1 - \frac{\eta}{2}\right) M_{jk}(v) + \frac{\eta}{2} M_{jk}(v + U) \right]. \quad (22)$$

Eqs. (22) and (17) provide the analytical forms of the conductance matrices in terms of the gate potential v_s and v , respectively. In order to express the xc kernel matrix \mathbf{F}_{xc} as functional of the density, we still need to express these gate potentials in terms of the density. The interacting (non-interacting) gate-density relation $v(n)$ ($v_s(n)$) is obtained by numerically inverting the density-potential relationship obtained by inserting the spectral function Eq. (14) (Eq. (15)) into Eq. (13a). From Eq. (11), the xc kernel matrix can then be expressed solely in terms of the density as

$$\mathbf{F}_{xc}(n) = \mathbf{L}_s(v_s(n))^{-1} - \mathbf{L}(v(n))^{-1}. \quad (23)$$

In order to complete our DFT scheme we need to provide an approximation for the Hxc (gate) potential $v_{\text{Hxc}}(n)$ to be used in Eq. (11). In the present work we use the Hxc potential of the single site model²⁹ (SSM) with an effective temperature T^* as proposed in Ref. 44 in order to correctly account for the dependence on the coupling. We will refer to this scheme as T^* DFT. In particular, we replace the effective temperature of Ref. 44 with

$$T^*(T, \gamma, U) = \frac{T^2 + \eta(\gamma, U, T)\gamma T + \eta^2(\gamma, U, T)\gamma^2}{T + \eta(\gamma, U, T)\gamma}, \quad (24a)$$

$$\eta(\gamma, U, T) = \eta_1(\gamma/T)\eta_2(U/T), \quad (24b)$$

$$\eta_1(x) = 0.478x^{-\frac{1}{2}} + 0.1331, \quad (24c)$$

$$\eta_2(x) = 0.676 \arctan(0.064x) + 0.661. \quad (24d)$$

To assess the accuracy of the proposed analytical Hxc functional, we compare it against the numerically exact inversion or reverse-engineered (RE) Hxc functional. This is computed as the difference between the numerically inverted interacting and non-interacting gate potentials from Eqs. (13) and (16) at equilibrium. We have

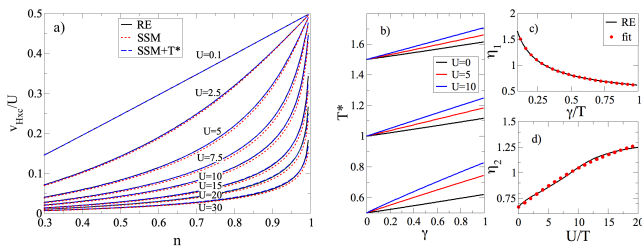


FIG. 2. a) Comparison of the reverse engineered (RE) Hxc potential from the many-body model with the one of the single-site model (SSM) and the SSM corrected with the effective temperature Eq. (24) for different Coulomb interactions and $\gamma/T = 0.1$. b) Effective temperature T^* for $T = 0.5, 1, 5$ as function of the coupling γ . c) and d) Comparison between the rate equation fitting functions η_1 and η_2 and the parametrizations of Eqs. (24c) and (24d).

found that the above expressions, with a fit for the numerical values in Eqs. (24c) and (24d), correct the standard DFT results and bring them closer to the MBM for the SIAM.

In Fig. 2 a) we compare the Hxc potential v_{Hxc} from reverse-engineerings of our many-body model with the SSM Hxc potential (no coupling) and the SSM Hxc potential with effective temperature to take into account the coupling for different values of the Coulomb interaction. The correction induced by the effective temperature for different couplings (Fig. 2 b)) produces a small variation in the Hxc potential which is essential to capture the correct strong-interaction limit of the thermoelectric efficiencies which will be presented in the next section. This dependence on subtle details of the Hxc functional is reminiscent of the ones observed in Ref. 45 for the description of the level occupation switching effect.

B. Results

In this section we present our numerical results. Here our interest lies in the description of the thermoelectric efficiency η as well as various linear-response transport coefficients of the quantum thermal machine for finite Coulomb interactions and multiple reservoirs, see Fig. 1 for $\mathcal{N} = 3$.

In order to access these quantities, we first solve the DFT problem in the standard way to obtain the density. Then, following the scheme presented in the previous section we compute the kernel matrix \mathbf{F}_{xc} , the linear response matrix \mathbf{L} and finally, through Eq. (5), the currents to linear order. The multi-terminal efficiency can then be obtained from the currents through^{6,18}

$$\eta = \frac{P}{\sum_{\alpha+} Q_{\alpha}} = \frac{\sum_{\alpha=1}^{\mathcal{N}} Q_{\alpha}}{\sum_{\alpha+} Q_{\alpha}} \quad (25)$$

where the symbol $\sum_{\alpha+}$ indicates that the sum is restricted to positive contributions of the heat currents.

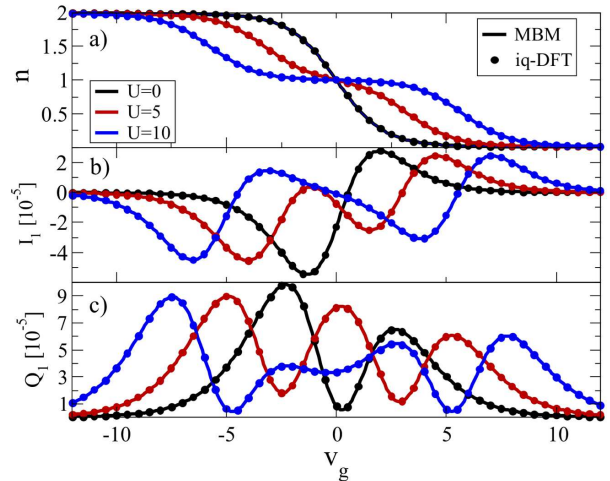


FIG. 3. Comparison of the density and currents I_1 and Q_1 from the reference MBM and iq-DFT as function of the gate voltage $v_g = v + \frac{U}{2}$ for different Coulomb interactions and $\mathcal{N} = 3$. The parameters used are $\gamma_i = \gamma/3 = 0.1T$, $V_1 = -V_2 = -5 \cdot 10^{-4}T$, $\Psi_1 = -\Psi_2 = 10^{-3}$ and $V_3 = \Psi_3 = 0$.

Eq. (25) is restricted to positive values of the output power P . In the following, we assume the condition $P > 0$ is always satisfied. Usually, this efficiency is presented normalized with its upper bound, the Carnot efficiency. The Carnot efficiency in turn is obtained by imposing zero entropy production $\dot{\mathcal{S}} = \frac{1}{T} \sum_{\alpha=1}^{\mathcal{N}-1} (I_{\alpha} V_{\alpha} + Q_{\alpha} \Psi_{\alpha}) = 0$ which leads to

$$\eta_C = \frac{\sum_{\alpha=1}^{\mathcal{N}-1} Q_{\alpha} (1 - \frac{T_N}{T_{\alpha}})}{\sum_{\alpha+} Q_{\alpha}}. \quad (26)$$

For the two terminal case one recovers the well known expression $\eta_C = 1 - T_2/T_1$.⁴⁶

In the following, unless explicitly noted, all energies are given in units of the temperature T . In Fig. 3 we present a comparison of the density and currents from the many-body model and iq-DFT. The small values used for the potentials $V_1 = -V_2 = -5 \cdot 10^{-4}T$, $\Psi_1 = 10^{-3}$ and $V_3 = \Psi_2 = \Psi_3 = 0$ ensure the applicability of the linear response equations for the currents Eq. (5). The agreement between MBM and iq-DFT is excellent both for the non-interacting as well as for the (strongly) correlated case, although the agreement may decrease away from the CB regime.

In Fig. 4 the thermoelectric efficiency is shown as function of the Coulomb interaction for $\gamma_i = \gamma/3 = 0.1T$, $v = 2T$. We observe that in the limit of very strong interaction the efficiency exactly corresponds to the non-interacting one. This can be understood from our many-body model, i.e., inserting the model spectral function of Eq. (14) into Eqs. (13). In the strong-interaction limit the contribution of the pole of the spectral function at $v + U$ is negligible for all “densities” due to the integral cutoff of the Fermi functions. Therefore, the density and

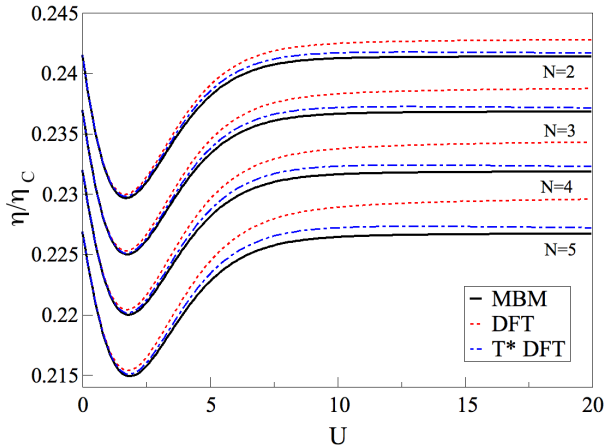


FIG. 4. Thermoelectric efficiency normalized by the Carnot efficiency as function of the Coulomb interaction for different number of leads $\mathcal{N} = 2, 3, 4, 5$. Comparison of the results of the many-body model (MBM) with iq-DFT results obtained with the original SSM Hxc potential of Ref. 29 (DFT) and those with the modified SSM using the effective temperature T^* of Eq. (24) (T^* DFT). The parameters are $\gamma_i = \gamma/3 = 0.1T$, $v = 2$, $V_1 = -5 \cdot 10^{-4}T$, $V_i = -V_1/(\mathcal{N} - 2)$ for $i = 2, \dots, \mathcal{N}-1$, $\Psi_1 = 10^{-3}$, $\Psi_i = -\Psi_1/(\mathcal{N}-2)$ for $i = 2, \dots, \mathcal{N}-1$ and $\Psi_{\mathcal{N}} = V_{\mathcal{N}} = 0$.

currents in this limit can be rewritten as

$$n_{U \rightarrow \infty} = \frac{n^s(v, \Phi)}{1 + \frac{1}{2}n^s(v, \Phi)} \quad (27a)$$

$$I_{U \rightarrow \infty} = I^s(v, \Phi)(1 - \frac{1}{2}n^s(v, \Phi)) \quad (27b)$$

$$Q_{U \rightarrow \infty} = Q^s(v, \Phi)(1 - \frac{1}{2}n^s(v, \Phi)), \quad (27c)$$

where $n^s(v, \Phi)$, $I^s(v, \Phi)$ and $Q^s(v, \Phi)$ are the non-interacting expressions of Eq. (16) evaluated at gate v and potentials Φ . Eq. (27) explicitly shows that in the strong-interacting limit, the interacting density and currents are fully determined by their non-interacting versions evaluated at the interacting potentials. Inserting Eq. (27) into Eq. (25) one finds that the prefactor $(1 - \frac{1}{2}n^s(v, \Phi))$ cancels out and we recover the efficiency of the non-interacting limit. For the parameters studied, in Fig. 4 the efficiency decreases as the Coulomb interaction is increased, finding the minimum around $U \sim 2$. Then it increases again up to the non-interacting value. The correction of the effective temperature of Eq. (24) is relevant in the strong-interacting limit: while with the original SSM parametrization of the Hxc potential, in the strongly correlated limit the efficiency does not approach the MBM limit, with the new parametrization it does. Our T^* -DFT results agree well with the MBM results in the region of parameters we investigated. We point out that the small deviation between T^* -DFT and MBM, in Fig. 4 stems from similar discrepancies in the heat and

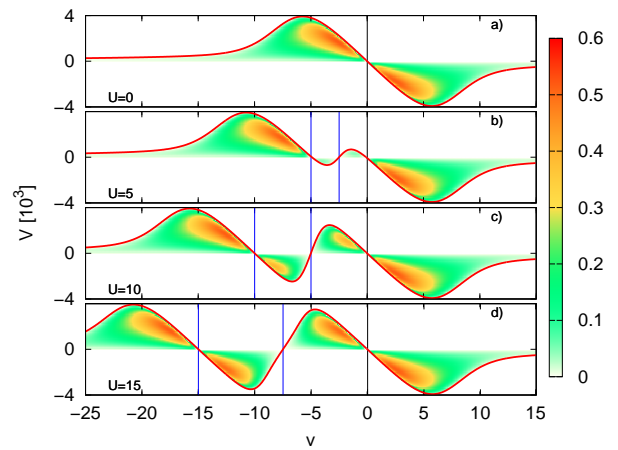


FIG. 5. Thermoelectric efficiency normalized by Carnot efficiency as function of the gate level and the bias potential V for the configuration $V_1 = -V_2 = V$, $V_3 = 0$, $\Psi_1 = -\Psi_2 = 10^{-3}$, $\Psi_3 = 0$ and parameters $\gamma_1 = \gamma_2 = \gamma_3 = 0.1T$. From a) to d) the Coulomb interaction is $U = 0, 5, 10, 15$. The red line corresponds to the open circuit voltage V_{oc} and the blue vertical lines correspond to the gate values $v = -U/2, -U$ at which $V_{oc} = 0$.

electrical currents, which are difficult to detect in Fig. 3.

In Fig. 5, the efficiency is calculated for $\mathcal{N} = 3$ as function of the gate v and bias V for the configuration $V_1 = -V_2 = V$, $V_3 = 0$, $\Psi_1 = -\Psi_2 = 10^{-3}$, $\Psi_3 = 0$ and different values of the Coulomb interaction $U/T = 0, 5, 10, 15$ from a) to d), respectively. The red line represents the open-circuit voltage V_{oc} , and corresponds to the bias at which the output power is zero, which in our configuration corresponds to the bias at which $I_1 = I_2$.

In Fig. 5a) the (iq-DFT) efficiency is presented for the three terminal setup in the non-interacting case. As in the two terminal case⁴⁷, the efficiency acts as a power generator for voltages $V_{oc} < V < 0$ (region 1) if the gate is negative and for voltages $0 < V < V_{oc}$ (region 2) if the applied gate is positive, and the open circuit voltage only vanishes at $v = 0$. The application of a finite Coulomb interaction in the QD (Fig. 5b),c) and d)) produces two new regions (where the QD acts as a power generator) that emerge in between regions 1 and 2. While the shape of regions 1 and 2 remain unchanged, region 1 is shifted to $v - U$. The new regions at finite U appear at $V_{oc} < V < 0$, $-U < v < -U/2$ (region 3) and $0 < V < V_{oc}$, $-U/2 < v < 0$ (region 4). The gate values at which there is a new transition between the regions is represented by the blue lines in the plots and correspond to the new gates at which the open circuit voltage vanishes $v = -U/2, -U$. As the Coulomb interaction is increased, the area of regions 3 and 4 increases and so the value of the efficiency inside these regions. In the high interaction limit the regions 1 and 3 and the regions 2 and 4 become equivalent, recovering the non-interacting limit around the Fermi energy. The same behavior has

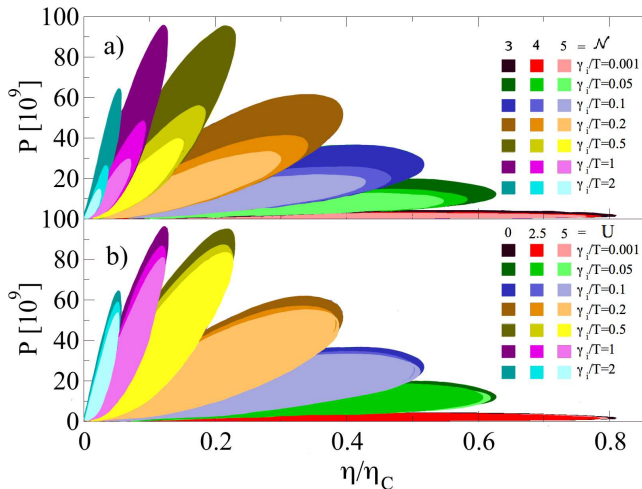


FIG. 6. Output power, in atomic units, as function of the efficiency for different total coupling strength γ and a) different number of reservoirs for the non-interacting QD, $U = 0$ and b) different Coulomb interactions U for the three terminal case $\mathcal{N} = 3$. Each solid region is obtained by scanning all the possible gate and bias combinations where the QD acts as a thermoelectric generator. The bias configuration selected corresponds to $V_1 = -(\mathcal{N} - 1)V_i$ with $i = 1, \dots, \mathcal{N} - 1$ and $V_{\mathcal{N}} = 0$.

been observed when the number of leads is $\mathcal{N} > 3$ (not shown).

We now focus our attention on the influence of the total coupling γ on the output power P and the efficiency η . The application of a bias inside the regions previously defined for different gates, results in a loop of the output power as function of the bias.⁴⁸ Scanning of all possible gates fills up the regions shown in Fig. 6. We observe that for the different numbers of leads studied here (Fig. 6 a)), the efficiency always approaches the Carnot efficiency as the coupling strength is reduced since the transmission function in this case approaches a delta function.^{48,49} On the other hand, when the coupling strength is increased, the number of electrons which contribute to the power generation increase, and, therefore, the output power reaches its maximum around $\gamma_{max} \sim 0.5T$. For couplings larger than γ_{max} , the transmission function $\mathcal{T}_{\alpha\alpha'}(\omega) = \gamma_\alpha\gamma_{\alpha'}/\gamma A(\omega)$ in Eq. (16) allows more energy states to contribute, in particular some negative contributions of the difference $\tilde{f}_\alpha(\omega) - \tilde{f}_{\alpha'}(\omega)$ which decrease the output power. It is worth noting that the larger the coupling to the leads, the larger the ratio between the \mathcal{N} and $\mathcal{N} + 1$ regions areas becomes. In Fig. 6 b) the thermoelectric efficiency is presented for different values of the Coulomb interaction and several coupling strengths. For small values of the coupling to the leads, the efficiency decreases as the interaction is applied and then it increases again tending to the non-interacting value, while the output power remains essentially unchanged. For larger values of the coupling, the efficiency remains

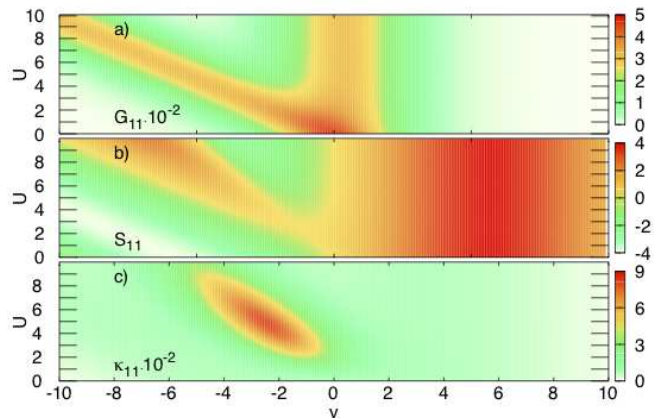


FIG. 7. Transport coefficients G_{11} , S_{11} , and κ_{11} as function of the Coulomb interaction and the gate level for $\mathcal{N} = 3$. The coupling strengths considered are $\gamma = 3\gamma_i = 0.1T$. All quantities expressed in atomic units.

mostly unchanged while the output power starts to decrease with the interaction.

To conclude our multi-terminal study of the quantum machine, we apply our formalism to calculate the transport coefficients and the figure of merit for the case $\mathcal{N} = 3$ and equal couplings γ_i . In Fig. 7 we show the transport coefficients G_{11} , S_{11} , κ_{11} as function of the Coulomb interaction and the gate level following the definitions of these coefficients derived in Ref. 18. Note that from these definitions, in the symmetric coupling setup $\gamma_1 = \gamma_2 = \gamma_3$ one can analytically show that $G_{11} = G_{22}$, $S_{11} = S_{22}$, $\kappa_{11} = \kappa_{22}$ while all the other off-diagonal transport coefficients vanish.

The electrical conductance (Fig. 7 a)) $G_{11} = G_{22}$ is maximum in the non-interacting case for the gate $v = 0$. At finite U , as expected, this feature splits in two Coulomb blockade peaks at $v = 0$ and at $v = -U$, a direct consequence of the form of the MBM spectral function of Eq. (14).

The Seebeck coefficient S_{11} (Fig. 7 b)) presents two main features which evolve with the Coulomb interaction: at negative gates $-10 - U < v < -U$ the Seebeck coefficient has its minimum and at positive gates $0 < v < 10$ the Seebeck coefficient evolves to its maximum value. For strong correlations $U/T \gtrsim 5$, a new feature appears between the other two structures alternating positive and negative contributions. Finally, the thermal conductance κ_{11} shows a localized structure distributed along gates $v \approx -U/2$ and reaching its maximum around $U \sim 5$, see Fig. 7 c).

The figure of merit in the multi-terminal setup can be evaluated from

$$ZT_{ij} = \frac{TG_{ij}^2 S_{ij}}{\kappa_{ij}}. \quad (28)$$

In Fig. 8 the diagonal element of the figure of merit is presented as function of Coulomb interaction and gate

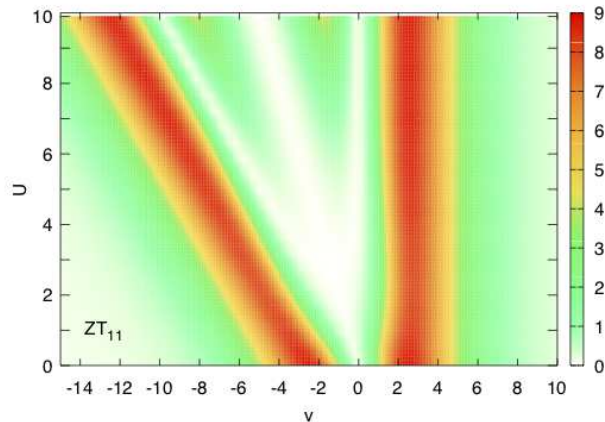


FIG. 8. Diagonal element of the figure of merit as function of the Coulomb interaction and the gate level for $\mathcal{N} = 3$. The coupling strengths considered are $\gamma = 3\gamma_i = 0.1T$

level. $ZT_{11} = ZT_{22}$ is mostly dominated by $S_{11} = S_{22}$. It shows two stripe regions centered at $v = -2.5 - U, 2.5$ where the figure of merit is maximized.

IV. CONCLUSIONS

In this work we generalize the iq-DFT theory for the description of electronic and thermal transport through nanoscale junctions connected to an arbitrary number of electrodes. The theory is established under a one-to-one correspondence between the set of “densities” $(n, I_1, Q_1, \dots, I_{\mathcal{N}-1}, Q_{\mathcal{N}-1})$ and the set of “potentials” $(v, V_1/T, \Psi_1/T, \dots, V_{\mathcal{N}-1}/T, \Psi_{\mathcal{N}-1}/T)$ in a finite domain

around the equilibrium state. The KS system requires $2(\mathcal{N} - 1)$ xc potentials which need to be parametrized.

We derived the linear response of the (multi-terminal) formalism finding formally exact expressions for the linear response electrical and heat currents, the figure of merit, the thermoelectric efficiency and the many-body transport coefficients, i.e., the electrical conductances, the Seebeck coefficients, as well as the thermal conductances. These quantities are fully and exactly expressed purely in terms of quantities accessible to the iq-DFT framework, i.e., the xc kernel matrix \mathbf{F}_{xc} and the Hxc potential $v_{\text{Hxc}}(n)$.

We applied the framework to an interacting quantum thermal machine with three, four and five reservoirs in the linear response and the Coulomb Blockade regime. We constructed the xc kernel matrix from reverse engineering of a many-body model, finding excellent agreement with the the reference many-body results for the currents and the transport coefficients as well as thermoelectric efficiency. We have found and identify the regions where the system acts as a thermal generator for different Coulomb interactions and analyzed these regions against the output power for several couplings to the leads and different number of reservoirs. Moreover, we understood analytically that in the strong-interaction limit the thermoelectric efficiency exactly corresponds to the non-interacting one.

V. ACKNOWLEDGMENTS

We acknowledge financial support through Grant PID2020-112811GB-I00 funded by MCIN/AEI/10.13039/501100011033 as well as by grant IT1453-22 “Grupos Consolidados UPV/EHU del Gobierno Vasco”.

* nahualcsc@dipc.org

† roberto.dagosta@ehu.es

‡ stefan.kurth@ehu.es

¹ G. Cuniberti, G. Fagas, and K. Richter, *Introducing Molecular Electronics* (Springer, Heidelberg, 2005).

² J. C. Cuevas and E. Scheer, *Molecular Electronics: An Introduction to Theory and Experiment* (World Scientific, London, 2010).

³ H. J. Goldsmid, *Introduction to Thermoelectricity* (Springer, Berlin, 2010).

⁴ R. Sánchez and M. Büttiker, *Phys. Rev. B* **83**, 085428 (2011).

⁵ G. Benenti, G. Casati, K. Saito, and R. S. Whitney, *Phys. Rep.* **694**, 1 (2017).

⁶ P. A. Erdman, F. Mazza, R. Bosisio, G. Benenti, R. Fazio, and F. Taddei, *Phys. Rev. B* **95**, 245432 (2017).

⁷ B. Sothmann, R. Sánchez, and A. N. Jordan, *Nanotechnology* **26**, 032001 (2014).

⁸ R. S. Whitney, *Phys. Rev. Lett.* **112**, 130601 (2014).

⁹ K. Esfarjani, M. Zebarjadi, and Y. Kawazoe, *Phys. Rev. B* **73**, 085406 (2006).

¹⁰ P. A. Jacquet, *J. Stat. Phys.* **134**, 709 (2009).

¹¹ O. Entin-Wohlman, Y. Imry, and A. Aharony, *Phys. Rev. B* **82**, 115314 (2010).

¹² D. Sánchez and L. Serra, *Phys. Rev. B* **84**, 201307(R) (2011).

¹³ J.-H. Jiang, O. Entin-Wohlman, and Y. Imry, *Phys. Rev. B* **85**, 075412 (2012).

¹⁴ K. K. Saha, W. Lu, J. Bernholc, and V. Meunier, *J. Chem. Phys.* **131**, 164105 (2009).

¹⁵ B. Sothmann and M. Büttiker, *Europhys. Lett.* **99**, 27001 (2012).

¹⁶ K. Brandner, K. Saito, and U. Seifert, *Phys. Rev. Lett.* **110**, 070603 (2013).

¹⁷ V. Balachandran, G. Benenti, and G. Casati, *Phys. Rev. B* **87**, 165419 (2013).

¹⁸ F. Mazza, R. Bosisio, G. Benenti, V. Giovannetti, R. Fazio, and F. Taddei, *New J. Phys.* **16**, 085001 (2014).

- ¹⁹ M. Büttiker, Y. Imry, R. Landauer, and S. Pinhas, Phys. Rev. B **31**, 6207 (1985).
- ²⁰ M. Büttiker, Phys. Rev. Lett. **57**, 1761 (1986).
- ²¹ Y. Meir and N. S. Wingreen, Phys. Rev. Lett. **68**, 2512 (1992).
- ²² W. Kohn and L. J. Sham, Phys. Rev. **140**, A1133 (1965).
- ²³ N.D. Lang, Phys. Rev. B **52**, 5335 (1995).
- ²⁴ M. D. Ventra, S.T. Pantelides, and N.D. Lang, Phys. Rev. Lett. **84**, 979 (2000).
- ²⁵ J. Taylor, H. Guo, and J. Wang, Phys. Rev. B **63**, 245407 (2001).
- ²⁶ M. Brandbyge, J.-L. Mozos, P. Ordejón, J. Taylor, and K. Stokbro, Phys. Rev. B **65**, 165401 (2002).
- ²⁷ B. K. Nikolić, K. K. Saha, T. Markussen, and K. S. Thygesen, J. Comput. Electron. **11**, 78 (2012).
- ²⁸ M. Thoss and F. Evers, J. Chem. Phys. **148**, 030901 (2018).
- ²⁹ G. Stefanucci and S. Kurth, Phys. Rev. Lett. **107**, 216401 (2011).
- ³⁰ J. P. Bergfield, Z.-F. Liu, K. Burke, and C. A. Stafford, Phys. Rev. Lett. **108**, 066801 (2012).
- ³¹ P. Tröster, P. Schmitteckert, and F. Evers, Phys. Rev. B **85**, 115409 (2012).
- ³² K. Yang, E. Perfetto, S. Kurth, G. Stefanucci, and R. D'Agosta, Phys. Rev. B **94**, 081410(R) (2016).
- ³³ G. Stefanucci and S. Kurth, Nano Lett. **15**, 8020 (2015).
- ³⁴ S. Kurth and G. Stefanucci, Phys. Rev. B **94**, 241103(R) (2016).
- ³⁵ S. Kurth and G. Stefanucci, J. Phys. Condens. Matter **29**, 413002 (2017).
- ³⁶ D. Jacob and S. Kurth, Nano Lett. **18**, 2086 (2018).
- ³⁷ D. Jacob, G. Stefanucci, and S. Kurth, Phys. Rev. Lett. **125**, 216401 (2020).
- ³⁸ N. Sobrino, S. Kurth, and D. Jacob, Phys. Rev. B **102**, 035159 (2020).
- ³⁹ S. Kurth, D. Jacob, N. Sobrino, and G. Stefanucci, Phys. Rev. B **100**, 085114 (2019).
- ⁴⁰ N. Sobrino, F. Eich, G. Stefanucci, R. D'Agosta, and S. Kurth, Phys. Rev. B **104**, 125115 (2021).
- ⁴¹ N. Sobrino, *Density Functional Theory for Steady-State Thermoelectric Transport with Applications to Strongly Correlated Systems*, Ph.D. thesis, Universidad del País Vasco (2021).
- ⁴² H. Haug and A.-P. Jauho, *Quantum Kinetics in Transport and Optics of Semiconductors*, Vol. 2 (Springer, New York, 2008).
- ⁴³ M. Abramowitz and I. Stegun, *Handbook of Mathematical Functions* (Dover, New York, 1965).
- ⁴⁴ N. Sobrino, R. D'Agosta, and S. Kurth, Phys. Rev. B **100**, 195142 (2019).
- ⁴⁵ N. Sobrino, D. Jacob, and S. Kurth, Phys. Rev. B **106**, 195124 (2022).
- ⁴⁶ M. T. Mitchison, Contemp. Phys. **60**, 164 (2019).
- ⁴⁷ N. Nakpathomkun, H. Q. Xu, and H. Linke, Phys. Rev. B **82**, 235428 (2010).
- ⁴⁸ M. Josefsson, A. Svilans, A. M. Burke, E. A. Hoffmann, S. Fahlvik, C. Thelander, M. Leijnse, and H. Linke, Nat. Nanotechnol. **13**, 920 (2018).
- ⁴⁹ T. E. Humphrey, R. Newbury, R. P. Taylor, and H. Linke, Phys. Rev. Lett. **89**, 116801 (2002).